Chinese Science Bulletin 2005 Vol. 50 No. 13 1309—1314

Antireflective characteristics of hemispherical grid grating

REN Zhibin[1], JIANG Huilin[1], LIU Guojun[1] & SUN Qiang[2]

1. State Key Laboratory on High Power Semiconductor Lasers, Changchun University of Science and Technology, Changchun 130022, China;
2. State Key Laboratory of Applied Optics, Changchun Institute of Optics, Fine Mechanics and Physics, Chinese Academy of Sciences, Changchun 130033, China

Correspondence should be addressed to Ren Zhibin (email: ren_zb@yahoo.com.cn)

Abstract **In this paper, the optical characteristics of new type hemispherical grid subwavelength grating are studied by using multi-level column structure approximation and rigorous coupled-wave analysis. This kind of grating could be fabricated by chemical methods, thus simplifying the fabrication technology of subwavelength gratings for visible light. By computer simulation and calculation, the hemispherical grid subwavelength gratings are proved to have antireflective characteristics. Two design schemes of this kind of grating are presented. In the first scheme, the grating could achieve a reflectivity as low as 3.4416×10^{-7}, which can be adapted to 0.46—0.7 μm of visible waveband and ±12° incident angle field. In the second scheme, the grating can achieve a reflectivity as low as 3.112×10^{-4} and adapted to the whole visible waveband and ±23° incident angle field. The application field of the latter scheme is wider than that of the former. The results of this paper could provide reference for the applications of the hemispherical grid subwavelength gratings for the visible waveband.**

Keywords: hemispherical grid subwavelength gratings, rigorous coupled-wave theory, antireflection, vector diffractive analysis, visible waveband.

DOI: 10.1360/982004-145

Subwavelength surface-relief gratings whose periods are smaller than incident wavelength have antireflective characteristics[1−4]. People could etch the surface of an optical element or a substrate to fabricate subwavelength surface relief grating to acquire low reflectivity; therefore, the grating could take the place of conventional optical thin films. Because the material of the surface relief grating is the same as its substrate, the stability of the grating is better than that of the conventional optical thin film and the localization of limited material of thin films is avoided. At present, the surface relief pattern generated by electron beam lithography, laser direct writing lithography or photomask exposure, etc. have been transferred to the surface of an optical element through replication or reactive ion etching to fabricate subwavelength antireflective gratings[5−14]. Now the fabrication technology of subwavelength gratings for microwave and infrared is mature. However, the pattern exposure and transferring procedure of the subwavelength gratings for visible light is not easy to control and fabricate and the fabrication takes much time. Recently, monolayer colloidal spherical microparticle arrays have been fabricated using chemical methods, whose diameters range from 0.02 to 10 μm[15]. Moreover, colloidal stamps, which are the duplicate negatives of the microparticle arrays, have been made and the two-dimensional demitional hemispherical subwavelength surface relief gratings could be generated on the surfaces of optical elements by using a sol-gel technology to transfer the surface shape of the colloidal stamps onto the surface of optical elements[16−18]. As this technology can produce subwavelength gratings for visible light with fine quality and precision, it attracts the attention of more and more people and becomes a focus of research. In this paper, we use the rigorous coupled-wave theory to analyze the characteristics of the hemispherical grid subwavelength grating, which is approximated by the multi-level columned structure. Moreover, the relations between the antireflective characteristics of the new kind of subwavelength grating and the grating structure parameters are acquired. The results show that this kind of grating has fine antireflective characteristics.

1 The foundation of analysis model of hemispherical grid subwavelength grating and the rigorous coupled-wave analysis

The geometry structure of hemispherical grid subwavelength grating is shown in Fig. 1. To apply the rigorous coupled-wave analysis in our research, we use a multilevel column array structure shown in Fig. 2 to simulate the grating. In Fig. 2, we could assume that the radius of the hemisphere to be R, diameter of the hemisphere to be D, T to be the period of the grating, the depth of the lth level to be h_l and the radius of the lth level to be r_l .

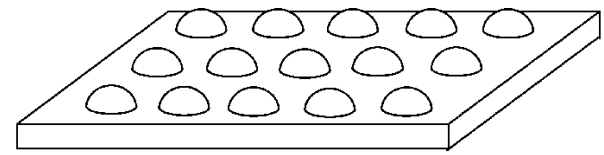

Fig. 1. A two-dimensional subwavelength grating with hemispherical grid.

To analyze the optical properties of the multi-level column array shown in Fig. 2, we take each level as a single step column array structure shown in Fig. 3 and apply boundary conditions between the connective levels.

We adopt the method illustrated in ref. [19] to analyze the lth level single step column array. In Fig. 3, the space is divided into three regions denoted by I, II and III. In regions I and III, the electric field of light wave is expressed in the form of a series of plane-wave. Let $\boldsymbol{k}_1$ and $\boldsymbol{u}$ be the wavevector and amplitude of electric field $\boldsymbol{E}^{\mathrm{i}}$ of the

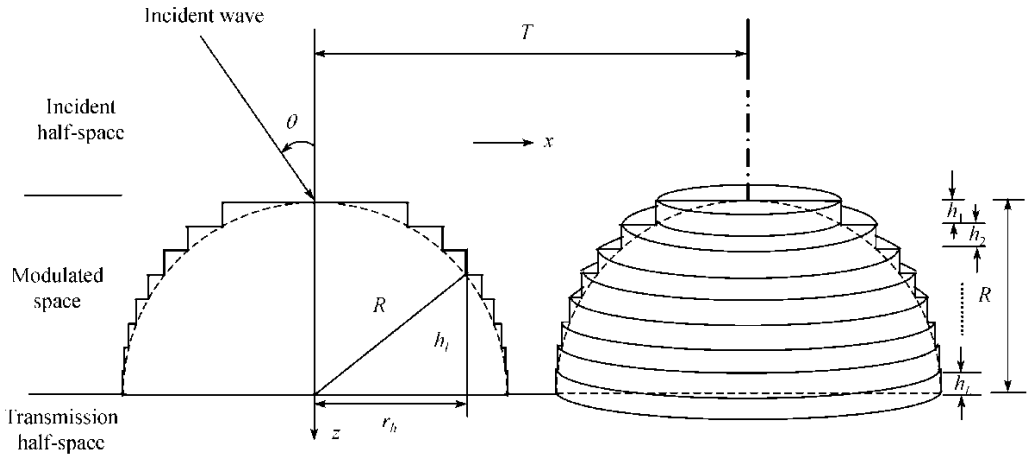

Fig. 2. Geometry of the multi-step column structure and the hemispherical subwavelength grating.

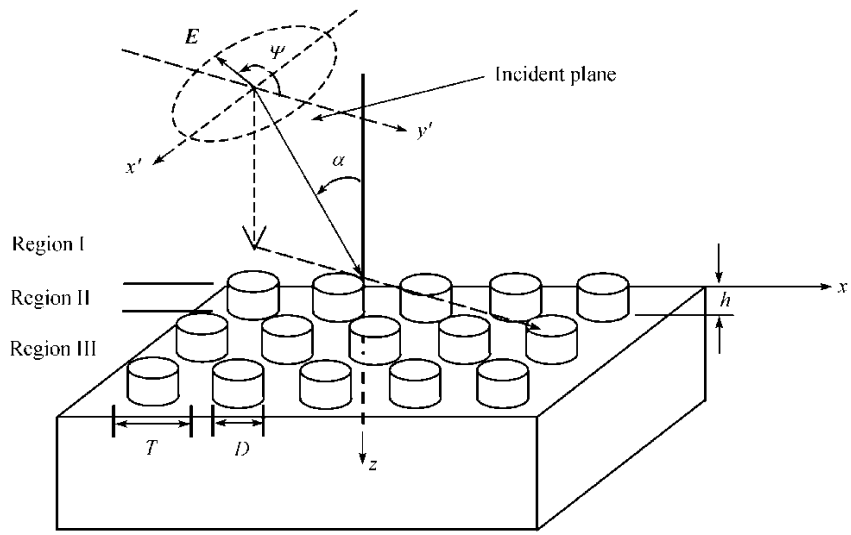

Fig. 3. Geometry of the 2-D columned grid array diffraction problem analyzed.

incident wave and $\boldsymbol{R}_{mn}$ and $\boldsymbol{T}_{mn}$ be the amplitude of the reflected waves with wavevector $\boldsymbol{k}_{1mn}$ and the transmitted waves with wavevector k_{3mn}, respectively. According to the Rayleigh expansions, the electric fields may be expressed as

$$\boldsymbol{E}^{\mathrm{I}} = \boldsymbol{E}^{\mathrm{i}} + \sum_{m=-\infty}^{\infty}\sum_{n=-\infty}^{\infty} \boldsymbol{R}_{mn} \times \exp(\mathrm{i}\boldsymbol{k}_{1mn} \times \boldsymbol{r}), \quad (1)$$

$$\boldsymbol{E}^{\mathrm{III}} = \sum_{m=-\infty}^{\infty}\sum_{n=-\infty}^{\infty} \boldsymbol{T}_{mn} \times \exp[\mathrm{i}\boldsymbol{k}_{3mn} \times (\boldsymbol{r} - \boldsymbol{h})], \quad (2)$$

where $\boldsymbol{E}^{\mathrm{i}}=\boldsymbol{u}\exp(\mathrm{i}\boldsymbol{k}_0 \cdot \boldsymbol{r})$.

According to the Maxwell equation, the magnetic field of incident wave, reflective wave and transmitted wave can be expressed as follows:

$$\boldsymbol{H}^{\mathrm{i}} = (\omega\mu_0)^{-1}\boldsymbol{k}_0 \times \boldsymbol{u}\exp(\mathrm{i}\boldsymbol{k}_0 \cdot r), \quad (3)$$

$$\boldsymbol{H}^{\mathrm{I}} = \boldsymbol{H}^{\mathrm{i}} + (\omega\mu_0)^{-1}\sum_{m=-\infty}^{\infty}\sum_{n=-\infty}^{\infty} \boldsymbol{k}_{1mn} \times \boldsymbol{R}_{mn}\exp(\mathrm{i}\boldsymbol{k}_{1mn} \cdot \boldsymbol{r}), \quad (4)$$

$$\boldsymbol{H}^{\mathrm{III}} = (\omega\mu_0)^{-1}\sum_{m=-\infty}^{\infty}\sum_{n=-\infty}^{\infty} \boldsymbol{k}_{3mn} \times \boldsymbol{T}_{mn}\exp[\mathrm{i}\boldsymbol{k}_{3mn} \cdot (\boldsymbol{r} - \boldsymbol{h})]. \quad (5)$$

In region II, the electric and magnetic fields of light wave are labeled as $\boldsymbol{E}^{\mathrm{II}}$ and $\boldsymbol{H}^{\mathrm{II}}$ and they can be expressed by the form of a series of space harmonic waves that only vary along z axis, i.e.

$$\boldsymbol{E}^{\mathrm{II}} = \sum_{m=-\infty}^{\infty}\sum_{n=-\infty}^{\infty} [E_{mn}^{x}(z)\boldsymbol{i} + E_{mn}^{y}(z)\boldsymbol{j}] \times \exp[\mathrm{i}(k_{xm}\boldsymbol{i} + k_{yn}\boldsymbol{j})], \quad (6)$$

$$\boldsymbol{H}^{\mathrm{II}} = \left(\frac{\varepsilon_0}{\mu_0}\right)^2 \sum_{m=-\infty}^{\infty}\sum_{n=-\infty}^{\infty}[H_{mn}^x(z)\boldsymbol{i} + H_{mn}^y(z)\boldsymbol{j}] \times \exp[\mathrm{i}(k_{xm}\boldsymbol{i} + k_{yn}\boldsymbol{j})]. \tag{7}$$

According to the Floquet theorem, there are only x component and y component in the grating modulation region (region II). So the wavevectors in eqs. (6) and (7) are

$$k_{xm} = k_{x0} + m2\pi / T_x, \tag{8}$$

$$k_{ym} = k_{y0} + n2\pi / T_y. \tag{9}$$

And the z components in regions I and III are

$$k_{zmn}^{\mathrm{I}} = \sqrt{k_0^2\varepsilon^{\mathrm{I}} - k_{xm}^2 - k_{yn}^2}, \tag{10}$$

$$k_{zmn}^{\mathrm{III}} = \sqrt{k_0^2\varepsilon^{\mathrm{III}} - k_{xm}^2 - k_{yn}^2}. \tag{11}$$

Because of the periodicity configuration of grating modulate region, the dielectric constant ε can be expanded in the Fourier series

$$\varepsilon(x,y,z) = \sum_{p=-\infty}^{\infty}\sum_{q=-\infty}^{\infty}\varepsilon_{pq}(z)\times\exp\left[\mathrm{i}\left(p\frac{2\pi}{T_x}x + q\frac{2\pi}{T_y}y\right)\right], \tag{12}$$

where

$$\varepsilon_{pq}(z) = \frac{1}{T_xT_y}\int_{-\frac{T_x}{2}}^{\frac{T_x}{2}}\int_{-\frac{T_y}{2}}^{\frac{T_y}{2}}\varepsilon \times\exp\left[-\mathrm{i}\left(p\frac{2\pi}{T_x}x + q\frac{2\pi}{T_y}y\right)\right]\mathrm{d}x\mathrm{d}y. \tag{13}$$

It is very important to solve the parameter ε_{pq} according to different grating profiles in the procedure of rigorous coupled-wave analysis and calculation. For the lth level column grid subwavelength grating, the expression of ε is

$$\varepsilon_l = \begin{cases}\varepsilon_1 & T_x/2 < x < T_x/2, T_y < y < T_y/2,\ x^2+y^2 > r_l^2,\\ \varepsilon_2 & x^2+y^2 < r_l^2.\end{cases} \tag{14}$$

Substituting eq. (14) into eq. (13), we have

$$\varepsilon_{pq}(z) = \begin{cases}\varepsilon_1 + \pi(\varepsilon_2-\varepsilon_1)\dfrac{r_l^2}{T_xT_y}, & \rho=0;\\ \dfrac{r_l(\varepsilon_2-\varepsilon_1)\cdot J_l(2\pi r_l\rho)}{\rho T_xT_y}, & \rho\neq 0.\end{cases} \tag{15}$$

where $J_l(2\pi r\rho)$ is Bessel J function and $\rho = \left[\left(\frac{p}{T_x}\right)^2 + \left(\frac{q}{T_y}\right)^2\right]^{1/2}$.

Assume the time factor to be $\exp(-\mathrm{i}\omega t)$ and substitute eq. (13) and electric field $\boldsymbol{E}^{\mathrm{II}}$ and magnetic field $\boldsymbol{H}^{\mathrm{II}}$ of region II into Maxwell equations set. Then according to Laurent law, we have

$$\frac{\partial E_{mn}^x}{\partial z} = \mathrm{i}k_0H_{mn}^y - \mathrm{i}(k_{xm}/k_0) \times\sum_{p=-\infty}^{\infty}\sum_{q=-\infty}^{\infty}\bar{\varepsilon}_{m-p,n-q}\times(k_{xp}H_{pq}^y - k_{yq}H_{pq}^x), \tag{16}$$

$$\frac{\partial E_{mn}^y}{\partial z} = -\mathrm{i}k_0H_{mn}^x - \mathrm{i}(k_{yn}/k_0) \times\sum_{p=-\infty}^{\infty}\sum_{q=-\infty}^{\infty}\bar{\varepsilon}_{m-p,n-q}\times(k_{xp}H_{pq}^y - k_{yq}H_{pq}^x), \tag{17}$$

$$\frac{\partial H_{mn}^x}{\partial z} = \mathrm{i}(k_{xm}/k_0)(k_{xm}E_{mn}^y - k_{yn}E_{mn}^x) - \mathrm{i}k_0\times\sum_{p=-\infty}^{\infty}\sum_{q=-\infty}^{\infty}\varepsilon_{m-p,n-q}\times E_{pq}^y, \tag{18}$$

$$\frac{\partial H_{mn}^y}{\partial z} = \mathrm{i}(k_{yn}/k_0)(k_{xm}E_{mn}^y - k_{yn}E_{mn}^x) + \mathrm{i}k_0\times\sum_{p=-\infty}^{\infty}\sum_{q=-\infty}^{\infty}\varepsilon_{m-p,n-q}\times E_{pq}^x. \tag{19}$$

To meet the boundary conditions, the tangential component of the electric and magnetic field should be continuous at the boundary of regions I, II, and III; that is, the electric field of eqs. (1) and (2) have the following relations at the positions of z=0 and z=h.

$$u_x\delta_{m0}\delta_{n0} + R_{mn}^x = E_{mn}^x(0), \tag{20}$$

$$u_y\delta_{m0}\delta_{n0} + R_{mn}^y = E_{mn}^y(0), \tag{21}$$

$$E_{mn}^y(h) = T_{mn}^y, \tag{22}$$

$$E_{mn}^x(h) = T_{mn}^x. \tag{23}$$

And according to Maxwell equations, the magnetic field has the following relations at the positions of z=0 and z=h:

$$\delta_{m0}\delta_{n0}(k_{y0}u_z - k_{z00}^{\mathrm{I}}u_y) + k_{yn}R_{mn}^z + k_{zmn}^{\mathrm{I}}R_{mn}^y = k_0H_{mn}^x(0), \tag{24}$$

$$\delta_{m0}\delta_{n0}(k_{z00}^{\mathrm{I}}u_x - k_{x0}u_z) - k_{xm}R_{mn}^z - k_{zmn}^{\mathrm{I}}R_{mn}^x = k_0H_{mn}^y(0), \tag{25}$$

$$k_0H_{mn}^y(h) = -k_{xm}T_{mn}^z + k_{zmn}^{\mathrm{III}}T_{mn}^x, \tag{26}$$

$$k_0H_{mn}^x(h) = k_{ym}T_{mn}^z - k_{zmn}^{\mathrm{III}}T_{mn}^y. \tag{27}$$

Maharam and Gaylord [20] have given the solutions of eqs. (16)—(19) which are composed of the eigenvalues and eigenvectors of a series of correlation coefficient matrixes, whose concrete forms are as follows:

$$E_{mn}^x = \sum_j C_j\omega_{mn,j}^1\exp(\lambda_j z), \tag{28}$$

$$E_{mn}^y = \sum_j C_j\omega_{mn,j}^2\exp(\lambda_j z), \tag{29}$$

$$H_{mn}^x = \sum_j C_j\omega_{mn,j}^3\exp(\lambda_j z), \tag{30}$$

$$H^{y}_{mn} = \sum_{j} C_j \omega^{4}_{mn,j} \exp(\lambda_j z). \tag{31}$$

Substitute eqs. (28)—(31) into eqs. (16)—(19). Then the characteristic equation with the following form is obtained, namely

$$\lambda\omega = A\omega, \tag{32}$$

where λ is a diagonal matrix composed of λ_j in eq. (28)—(31), ω is an eignvector matrix composed of $\omega^{l}_{mn,j}$ (l=1, 2, 3, 4) in eqs. (28)—(31) and A is a constant matrix.

Besides boundary conditions of each layer given by eqs. (20)—(27), each step should fulfill the special boundary conditions between layers, namely

$$E^{x}_{mn,l}(h_l) = E^{x}_{mn,l+1}(h_l), \tag{33}$$

$$E^{y}_{mn,l}(h_l) = E^{y}_{mn,l+1}(h_l), \tag{34}$$

$$H^{x}_{mn,l}(h_l) = H^{x}_{mn,l+1}(h_l), \tag{35}$$

$$H^{y}_{mn,l}(h_l) = H^{y}_{mn,l+1}(h_l), \tag{36}$$

where l = 1, 2, ⋯, L–1 denotes the layer to which the variable belongs. In the procedure of calculation, we have the relations

$$\begin{cases} A_1(h)C_1 = A_2(h)C_2, \\ A_2(2h)C_2 = A_3(2h)C_3, \\ \vdots \\ A_l(lh)C_l = A_l + l(lh)C_{l+1}, \\ \vdots \end{cases} \tag{37}$$

By recursion rule, we have

$$C_1 = A_1'(h)A_2(h)A_2'(2h)A_3(2h)\cdots A_{l-1}'(lh-h)A_l(lh)C_l. \tag{38}$$

From eq. (38), we know that C_l and the electromagnetic field of each level can be solved subsequently as long as the constant of the first layer C_1 and the expressions of constant matrix A_l of each level are given.

The diffraction efficiency of the reflected and transmitted waves may be given by the following expressions:

$$\eta^{\mathrm{I}}_{mn} = \mathrm{Re}(k^{\mathrm{I}}_{zmn} / k^{\mathrm{I}}_{z00}) \,|\, R_{mn} \,|^2, \tag{39}$$

$$\eta^{\mathrm{III}}_{mn} = \mathrm{Re}(k^{\mathrm{III}}_{zmn} / k^{\mathrm{III}}_{z00}) \,|\, T_{mn} \,|^2, \tag{40}$$

where Re denotes the real part of a variable, and $k_{\mathrm{I}zmn}$ and $k_{\mathrm{III}zmn}$ are the components of the wavevectors k_{1mn} and k_{3mn} in the z-direction, respectively. For a lossless grating, the permittivity $\varepsilon^{\mathrm{III}}$ is a real number and conservation of energy requires that

$$\sum_{m=-\infty}^{\infty} \sum_{n=-\infty}^{\infty} (\eta^{\mathrm{I}}_{mn} + \eta^{\mathrm{III}}_{mn}) = 1 \tag{41}$$

2 Analysis and design

After compiling matlab program using the formula above, we could carry through numerical calculations and study the optical characteristics of the hemispherical grid subwavelength grating. When the total number L of the steps is large enough ($L \geqslant 8$), the multi-step column structure may approximate the hemispherical grid grating with very little error. In this paper, we use a 16-level column structure to approximate the hemispherical grid surface-relief grating. As this kind of grating is often fabricated on a glass substrate, the refractive index of the grating n_s =1.5 and the refractive index of the surrounding media n_i=1 are adopted.

A hemispherical grid grating has two important structure parameters, period T and diameter D. To acquire fine antireflective characteristics over the whole visible waveband, we choose 0.55 μm as the center wavelength. After the effects of period T and diameter D on the reflectivity are determined and the minimum reflectivity is obtained, the minimum reflectivity and the value of period T and diameter D can be solved. The relation curve of the reflectivity, period T and D/T with parameters λ =0.55 μm and α =0° is shown in Fig. 4. From this figure, we could see that periods T and D/T have great effect on the reflectivity, and the low reflectivity that approaches 0 could be acquired by choosing appropriate parameters. From the numerical results it follows that the reflectivity decreases to the minimum of 3.4416×10^{-7} when T equals 0.45714 μm and D equals 0.348295 μm.

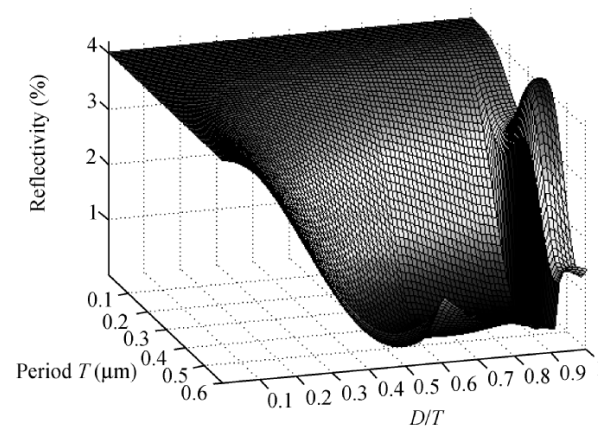

Fig. 4. Relation among reflectivity, T and D/T, with parameters: λ=0.55 μm, α =0°.

Now we analyze the antireflective characteristics of the grating over the whole visible waveband with parameters T=0.45714 μm and D=0.348295 μm. The relation curve of reflectivity and incident wavelength λ is shown in Fig. 5. From this figure we see that when incident wavelength varies from 0.46 to 0.7 μm the reflectivity is below 0.081% and the antireflective function is notable; however, in the range from 0.4 to 0.45 μm of the incident wavelength, reflectivity is above 2.5% and the antireflective effect is unapparent because the period of the grating is larger than that of the incident wavelength, and the grating is not subwavelength grating any more. However,

if we want to acquire good antireflective function in the waveband from 0.46 to 0.7 μm, the parameters T=0.45714 μm and D=0.348295 μm are optimal.

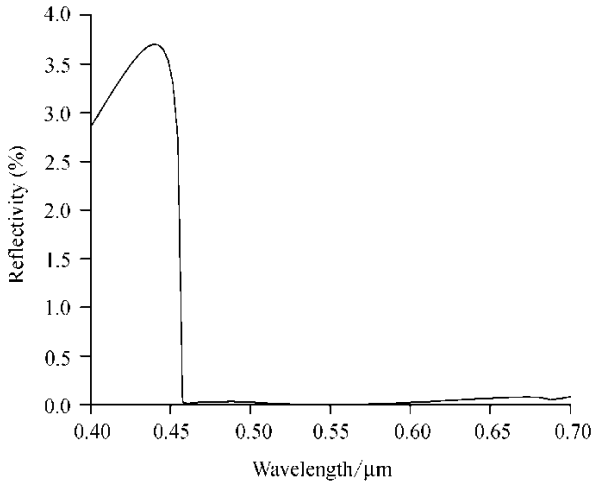

Fig. 5. Relation between reflectivity and the incident wavelength λ, with parameters: T=0.45714 μm, D=0.7619T, α=0°.

To acquire the subwavelength grating with fine antireflective characteristics over the whole visible waveband, the diameter and period have to be redesigned. A period of approximately 0.45714 μm is needed to obtain low reflectivity; however, the period should be smaller than 0.4 μm in order to realize low reflectivity in the shorter wavelength part of the visible waveband. Therefore, considering the two factors above, we choose 0.399 μm as the period to find the optimal value of the diameter. The relation curve of reflectivity and D/T with the parameter T=0.399 μm is shown in Fig. 6. From this figure, we see that the reflectivity arrives at the minimum of 3.112×10^{-4} with the parameters D=0.785T=0.3132 μm. Though this minimum is about 1000 times that of the first case, it could also satisfy the practical requirement.

Fig. 7 presents the reflectivity curves for this kind of gratings over the visible waveband with the parameters T=0.399 μm and D=0.785T. The reflectivity of the grating is below 0.35% over the whole visible waveband, satisfying the practical need.

Next, we study the variety regularity of reflectivity when the incident angle varies. Fig. 8 shows the variety regularity of the two gratings' reflectivity designed above when the incident angle varies. The numerical results show that the two gratings designed in this paper acquire a reflectivity as low as 0.2% when the incident angle varies in the region of ±12° and ±23°, respectively.

3 Conclusions

Using the rigorous coupled-wave theory, we studied the antireflective characteristics of the hemispherical grid

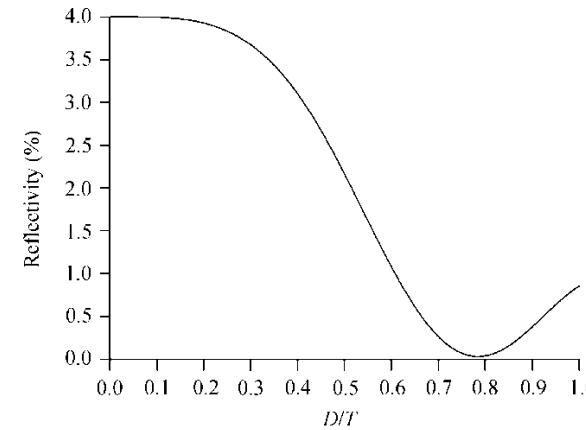

Fig. 6. Relation between reflectivity and D/T, with parameters λ =0.55 μm, T=0.399 μm, α=0°.

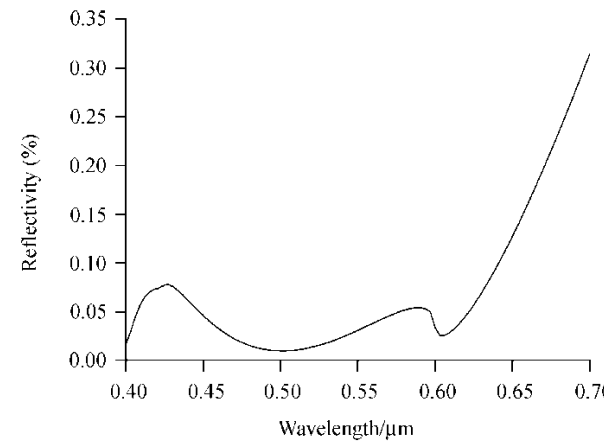

Fig. 7. Relation between reflectivity and the incident wavelength λ, with parameters T=0.399 μm, D =0.785T, α =0°

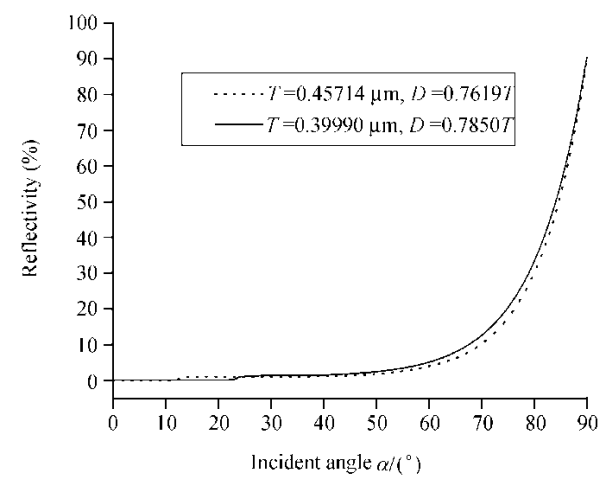

Fig. 8. Relation between reflectivity and the incident angle α, with parameter λ=0.55 μm.

subwavelength gratings. The numerical results are given by programming with matlab language, and two schemes are designed for visible wavebands. The first grating designed in this paper acquired a reflectivity as low as 3.4416×10^{-7} at a center wavelength of 0.55 μm with the incident angle variety region of ±12° and the second grating acquired a reflectivity as low as 3.112×10^{-4} with an incident angle variety region of ±23°. Though the second minimum reflectivity is 1000 times that of the first case, the difference is negligible in practical applications. When an optical system is strict with the reflectivity and not strict with the waveband and the incident angle, we choose the first scheme; however, the second scheme is more applicable for other instances. The results of this paper provide theoretic references for the application of the hemispherical grid subwavelength gratings for the visible waveband.

References

1. Grann, E. B., Moharam, M. G., Pommet, D. A., Artificial uniaxial and biaxial dielectrics with use of two-dimensional subwavelength binary gratings, J. Opt. Soc. Am. A, 1994, 11(10): 2695－2703.
2. Motamedi, M. E., Southwell, W. H., Gunning, W. J., Antireflection surface in silicon using binary optics technology, Appl. Opt., 1990, 31(22): 4372－4376.
3. Gaylord, T. K., Glytsis, E. N., Maharam, M. G., Zero-reflectivity homogeneous layers and high spatial-frequent surface-relief gratings on lossy materials, Appl. Opt., 1987, 26 (15): 3123－3135.
4. Cao, Z., Lu, Z., Li, F., Zhang, H., Sun, Q., Design consideration of two-dimensional anti-reflective subwavelength periodic gratings, Optics and Precision Engineering (in Chinese), 2002, 10(6): 537－541.
5. Pool, F. S., Wilson, D. W., Maker, P. D. et al., Fabrication and performance of diffractive optics for quantum well infrared photodetectors, Proc. SPIE, 1998, 3379: 402－409.
6. Schindler, A., Thomas, H., Dieter F. et al., Ion beam and plasma jet etching for optical component fabrication, Proc. SPIE, 2001, 4440: 217－227.
7. Urquhart, K. S., Stein, R., Lee, S. H., Computer-generated holograms fabricated by direct write of positive electron-beam resist, Optics Letter, 1993, 18(4): 308－310.
8. Lalanne, P., Michael, G. M., Design, fabrication and characterization of subwavelength periodic structures for semiconductor antireflection coating in the visible domain, Proc. SPIE, 1996, 2776: 300－309.
9. Malek, C. K., Hartley, F. T., Neogi, J., Focused ion beam direct micromachining of DOEs, Proc. SPIE, 2000, 4075: 167－172.
10. Kawamura, K., Sarukura, N., Hirano, M., Hosono, H., Fabrication of nonerasable gratings in SiO_2 glasses by a two-beam holographic method using infrared femtosecond laser pulses, Proc. SPIE, 2000, 4347: 195－206.
11. Schnabel, B., Kley, E.-B., Fabrication and application of subwavelength gratings, Proc. SPIE, 1997, 3008: 233－241.
12. Kanamori, Y., Sasaki, M., Hane, K., High-aspect-ratio two-dimensional silicon subwavelength gratings fabricated by fast atom beam etching, Proc. SPIE, 1999, 3874: 345－354.
13. Kuzmenko, P. J., Ciarlo, D. R., Stevens, C. G., Fabrication and testing of a silicon immersion grating for infrared spectroscopy, Proc. SPIE, 1994, 2266: 566－577.
14. Wiedemann, G. R., Dave, H. H., Jennings, D. E., Immersion grating and etched gratings for infrared astronomy, Proc. SPIE, 1994, 1946: 622－628.
15. Xia, Y., Gates, B., Yin, Y., Lu, Y., Monodispersed colloidal spheres: Old materials with new applications, Adv. Mater., 2000, 12(10): 693－713.
16. Sprenger, M., Walheim, S., Schafle, C., Steiner, U., Hierarchical pattern replication by polymer demixing, Adv. Mater., 2003,15(9): 703－706.
17. Xia, Y., Tien, J., Qin, D., Whitesides, G. M., Non-photolithographic methods for fabrication of elastomeric stemps for use in microcontact printing, Langmuir, 1996 12(16): 4033－4038.
18. Hirai, T., Hayashi, S., Lens functions of polymer microparticle arrays, Colloids and Surface A: Physiochemical and Engineering Aspects, 1999, 153: 503－513.
19. Zhang, D., Lu, Z., Yu, W., Li, F., Electromagnetic diffraction analysis of columned grid gratings, J. Opt. A: Pure Appl. Opt., 2002, 4(2): 180－186.
20. Maharam, M. G., Gaylord, T. K., Three-dimensional vector coupled-wave analysis of plannar-grating diffraction, J. Opt. Soc. Am., 1983, 73(5): 1105－1112.

(Received February 23, 2005; revised April 6, 2005)